

# Parameter Estimation by Density Functional Theory for a Lattice-gas Model of Br and Cl Chemisorption on Ag(100)

Tjipto Juwono, Ibrahim Abou Hamad, Per Arne Rikvold

*Department of Physics,  
Florida State University,  
Tallahassee, Fl 32306, USA*

Sanwu Wang

*Department of Physics & Engineering Physics,  
University of Tulsa,  
Tulsa, OK 74104, USA*

(Dated: September 3, 2018)

## Abstract

We study Bromine and Chlorine chemisorption on a Ag(100) surface, using a lattice-gas model and the quantum-mechanical Density Functional Theory (DFT) method. In this model the Br and Cl ions adsorb at the fourfold hollow sites of the Ag(100) surface, which can be represented by a square lattice of adsorption sites. Five different coverages were used for each kind of adsorbate. For each adsorbate and coverage, we obtained the minimum-energy configuration, its energy, and its charge distribution. From these data we calculated dipole moments, lateral interaction energies, and binding energies. Our results show that for Br the lateral interactions obtained by fitting to the adsorption energies obtained from the DFT calculation are consistent with long-range dipole-dipole lateral interactions obtained using the dipole moments calculated from the DFT charge distribution. For Cl we found that, while the long-range dipole-dipole lateral interactions are important, short-range attractive interactions are also present. Our results are overall consistent with parameter estimates previously obtained by fitting room-temperature Monte Carlo simulations to electrochemical adsorption isotherms [I. Abou Hamad et al., J. Electroanal. Chem. 554 (2003), 211; Electrochim. Acta 50 (2005), 5518].

## I. INTRODUCTION

The adsorption of halides on noble metals provides important model systems for studying adsorption on metal surfaces, particularly when there are ordered adsorbate structures. For this reason, these adsorption processes have been extensively studied [1, 2]. Adsorption of Bromine and Chlorine on metal has been the subject of many studies over the years. The systems we study here are Br and Cl chemisorbed on single-crystal Ag(100). Experimentally, Kleinherbers *et al.* [3] have found that the adsorption of Br, Cl, and I on Ag(100) surfaces in vacuum all resulted in the formation of a  $c(2 \times 2)$  overlayer with the adsorbates in the fourfold hollow sites. This implies a very strong, short-range repulsion, which we model as a nearest-neighbor exclusion [4].

The bonding of the adsorbates to the substrate and the surface electronic structures have been studied by Density Functional Theory (DFT) calculations. It is found that the bond between Br or Cl and the substrate is covalent with a polarization due to electron transfer from the substrate to the adsorbate [5–7]. The polarization results in dipole moments on the surface, which cause long-range dipole-dipole interactions between the adatoms.

Long-range dipole-dipole interactions have previously been incorporated in a lattice-gas model employed in room-temperature Monte Carlo simulation studies of the adsorbed system [8, 9]. In these works, the lateral interactions were extracted by fitting the results of the simulations to electrochemical adsorption isotherms. In the present study we instead estimate the lateral interactions by fitting the lattice-gas model to our DFT results.

We extract the next-nearest-neighbor lateral energy and the binding energy by fitting the lattice-gas model to the adsorption energies obtained from the DFT calculation. The same DFT calculation also yields charge distributions from which dipole-dipole interactions can be directly calculated. By comparing the two results, we examine the significance of the long-range dipole-dipole interactions within the lattice-gas model.

In this study we present DFT calculations using supercell models for the Ag(100) surfaces. The adsorbates in these DFT calculations are assumed to occupy a lattice of adsorption sites in accordance with a lattice-gas approximation [10]. The lattice-gas assumption of strongly located adsorbates is consistent with previous DFT calculations and dynamic Langevin-equation simulations for a continuum model [7].

The adsorption energies and charge distributions were calculated by DFT. We assume

long-range dipole-dipole interactions between the adsorbates, and we implement these long-range interactions in the fitting of the lattice-gas model to the adsorption-energy results and the dipole moments obtained from the DFT calculations.

Estimates of short-range lattice-gas interactions from DFT calculations of adsorption energies have also recently been performed for homoepitaxy [11–13] and heteroepitaxy [13] systems. However, these studies do not consider charge transfer and long-range interactions.

The rest of this paper is organized as follows. Section 2 describes the details of the DFT calculations and the methods used to analyze the results, Section 3 discusses the calculation of the dipole moment, Section 4 discusses the lattice-gas model, Section 5 presents the lattice-gas fitting, and Section 6 contains a discussion.

## II. DENSITY FUNCTIONAL THEORY

We applied DFT to obtain the ground-state energies and electron density functions for the adsorption of Br or Cl on a slab representing a Ag(100) surface. We prepared slabs with seven metal layers. Convergence checks with respect to the number of layers are discussed in Appendix A. The slab was placed inside a supercell with periodic boundary conditions. Two different sizes of supercells were examined. A  $2 \times 2$  supercell with the size of  $2a \times 2a \times 37.53\text{\AA}$ , and a  $3 \times 3$  supercell with the size of  $3a \times 3a \times 37.53\text{\AA}$ . Here,  $a = \alpha/\sqrt{2}$  where  $\alpha = 4.17\text{\AA}$  is the lattice constant of bulk Ag, which we obtained from DFT calculations by minimization of an Ag fcc structure. The  $2 \times 2$  supercell contained four surface Ag atoms on each side of the slab (28 Ag atoms in total), while the  $3 \times 3$  supercell contained nine surface Ag atoms on each side (63 Ag atoms in total).

The orientation of the surface normal defines the  $z$  direction. To maximize the symmetry, we distributed the adsorbates on both sides of the slab. One, two, and three Bromine or Chlorine atoms were placed on each  $3 \times 3$  surface to represent coverages  $\theta = 1/9$ ,  $2/9$ , and  $1/3$ , respectively. Two Bromine or Chlorine atoms were placed on each  $2 \times 2$  surface to represent  $\theta = 1/2$  and one to represent  $\theta = 1/4$ . Here the coverage  $\theta$  is defined as

$$\theta = \frac{1}{N_{\text{site}}} \sum_i c_i, \quad (1)$$

where  $c_i = 1$  when the site is occupied by the adsorbate, and  $c_i = 0$  otherwise. In other words, the coverage is the number of adsorbates divided by the total number of all possible

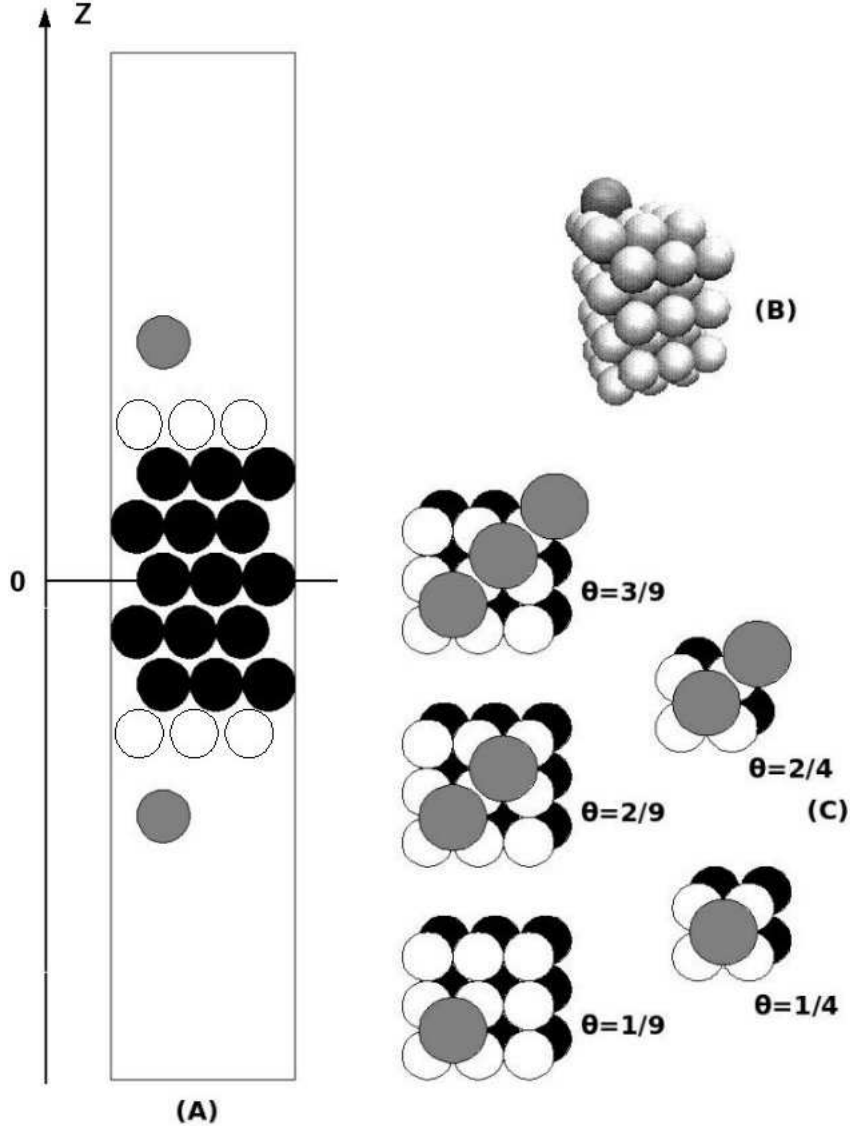


FIG. 1: (A) The cross section of the supercell, (B) a three-dimensional representation of the supercell, and (C) surface distributions of the adsorbates for various coverages. Adsorbate atoms: gray. Surface Ag atoms: white. Bulk Ag atoms: black.

adsorption sites,  $N_{\text{site}}$ . Figure 1 shows the cross section of a supercell and surface distributions of the adsorbate for various coverages. Due to the nearest-neighbor exclusion and the periodic boundary conditions the adsorbates can only be placed in diagonal positions, limiting  $\theta$  to less than or equal to  $1/2$ .

The calculations were performed by the DFT method using the Vienna Ab Initio Simulation Package (VASP) [14–16]. The basis set was plane-wave, with the generalized gradient-

corrected exchange-correlation functional [17, 18], Vanderbilt pseudopotentials [19, 20], and a cut-off energy of 400 eV. The  $k$ -point mesh was generated using the Monkhorst method [21] with a  $7 \times 7 \times 1$  grid for the  $2 \times 2$  supercells and a  $5 \times 5 \times 1$  grid for the  $3 \times 3$  supercells. To get to the configuration with minimum energy, we used a selective dynamics method, by which the ions in the top and bottom layers were allowed to relax in the  $z$  direction only, as opposed to the full dynamics in which the atoms would be allowed to move in all directions. This is the first step to avoid surface reconstruction, which is not expected to occur in this system under electrochemical conditions. The second step is to average the  $z$  coordinates of the top and bottom layers. The DFT results yield total energies and electron densities,  $\rho_e(\vec{x})$ .

We next ran static minimization on the resulting averaged minimum-energy structure. Here, ‘static’ means running energy minimization on the electron distribution without changing the positions of the nuclei. From this run, we obtained the total energy of the system,  $E_{\text{syst}}$ . We then took the same structure and removed the adsorbate to obtain the clean-slab structure. Again, we ran selective dynamics on this slab structure to obtain  $E_{\text{slab}}$ . To get the energy of an isolated halide atom, we also ran static minimization on an isolated halide atom to obtain  $E_{\text{hal}}$ . We define the adsorption energy per supercell per site as

$$E_{\text{ads}} = \frac{E_{\text{syst}} - E_{\text{slab}} - 2NE_{\text{hal}}}{2N_{\text{site}}}. \quad (2)$$

Here,  $N_{\text{site}}$  is the number of sites on one surface of the metal slab, and  $N$  is the number of halides on each side of the slab. In Fig. 2 we show  $E_{\text{ads}}$  as a function of  $\theta$  for both systems. We emphasize that  $E_{\text{ads}}$  contains the lateral interaction energy and is different from the single-particle binding energy  $E_{\text{b}}$ . The relation between these two quantities is given explicitly in Eq. (13) below.

To understand the surface polarization we need to study the charge-transfer behavior. We define the negative of the electron densities from the DFT output as the charge density distributions  $\rho(\vec{x})$ , and we introduce the charge transfer function per adsorbed atom, which is defined as follows [22]

$$\Delta\rho(\vec{x}) = \left[ \rho(\vec{x})_{\text{halide-Ag}(100)} - \sum_{i=1}^N \rho(\vec{x})_{\text{halide}} - \rho(\vec{x})_{\text{Ag}(100)} \right] / N, \quad (3)$$

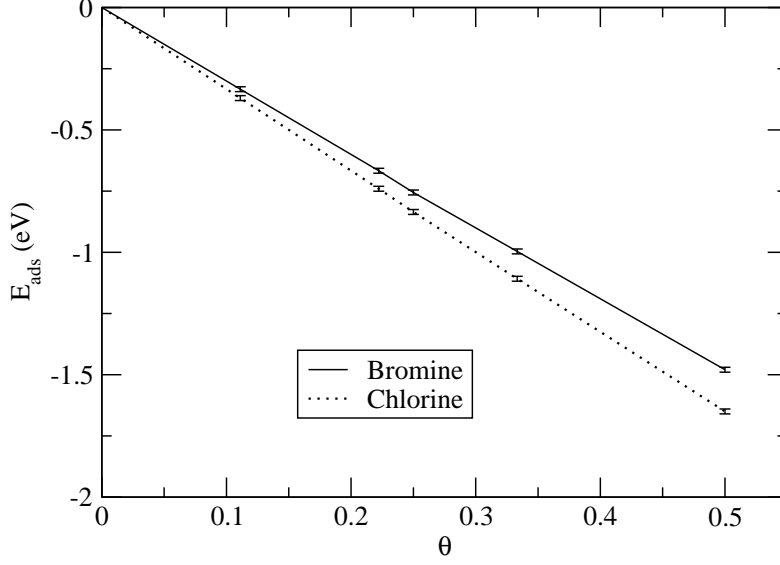


FIG. 2: Adsorption energy vs coverage. Despite the appearance on this scale, the lines are, in fact, slightly convex due to the repulsive lateral interactions. The “error bars” in this and subsequent figures do not represent statistical errors, but rather estimates of the accuracy of the results, based on the convergence studies discussed in Appendix A.

where  $\rho(\vec{x})_{\text{halide-Ag}(100)}$  is the full charge density of the adlayer system with  $N$  adsorbed Br or Cl on each side of the slab, and  $\rho(\vec{x})_{\text{halide}}$  is the full charge density of the pair of isolated halide atoms at the same positions as in the halide-Ag bonded system, and  $\rho(\vec{x})_{\text{Ag}(100)}$  is the charge density of the Ag(100) slab with all atoms at the same positions as in the halide-Ag bonded system [23]. After integrating over  $x$  and  $y$ , this yields the charge transfer function per pair of adsorbed atoms,

$$\Delta\rho(z) = [\rho(z)_{\text{halide-Ag}(100)} - N\rho(z)_{\text{halide}} - \rho(z)_{\text{Ag}(100)}]/N. \quad (4)$$

From the charge transfer function integrated over the  $x$  and  $y$  directions,  $\Delta\rho(z)$ , we can calculate the surface dipole moment as

$$p = \frac{1}{2} \int_{-h}^{+h} |z| \Delta\rho(z) dz. \quad (5)$$

Here  $h = \frac{1}{2}H$  where  $H$  is the height of the supercell. The zero point of the coordinate is placed at the middle of the supercell. Figure 3 shows the results of the dipole moment calculation for Bromine and Chlorine. Here we observe that the magnitude of the dipole moment decreases approximately linearly with  $\theta$ . The surface dipole moment of the energy-

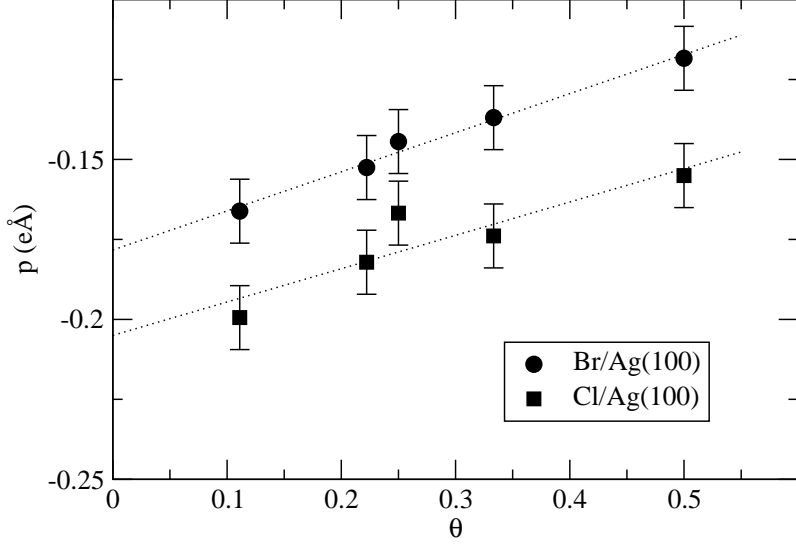


FIG. 3: Dipole moment vs coverage.

minimized clean slab was also calculated and verified to be the same as the surface dipole moment of the slab with all atoms at the same positions as in the halide-Ag bonded system, thus justifying our procedure.

Figure 4 shows the charge transfer function  $\Delta\rho(z)$  for Br/Ag(100) with  $\theta = 1/9$ . In this figure positive values indicate electrons being removed, while negative values indicate electrons being added. From the figure we see that charge is mostly transferred from the surface silver atoms to the adsorbates. Inside the bulk, the charge transfer function indicates only minor charge redistribution above and below each of the silver layers. Since the charge transfer function is calculated by subtracting the charge distributions of the clean slab and isolated adsorbate from that of the adsorbed system, we conclude that this small charge redistribution is caused by the adsorption processes.

Figure 5 shows the charge transfer function per adsorbed atom  $\Delta\rho(z)$  for Br/Ag(100) and Cl/Ag(100) for all coverages. Here we only show half of the supercell since the charge transfer function is symmetric in the  $z$  direction. Both systems show a similarity in that the magnitude and distribution of the charge transfer from the Ag surface are independent of the coverage. However, Fig. 5 also shows that while the magnitude of the charge transfer from the surface to the adsorbate is independent of the coverage, the resulting charge distribution around the adsorbate is not. Indeed, higher coverage results in a more asymmetrical charge distribution around the adsorbate. This asymmetry is more pronounced in the Br/Ag(100)

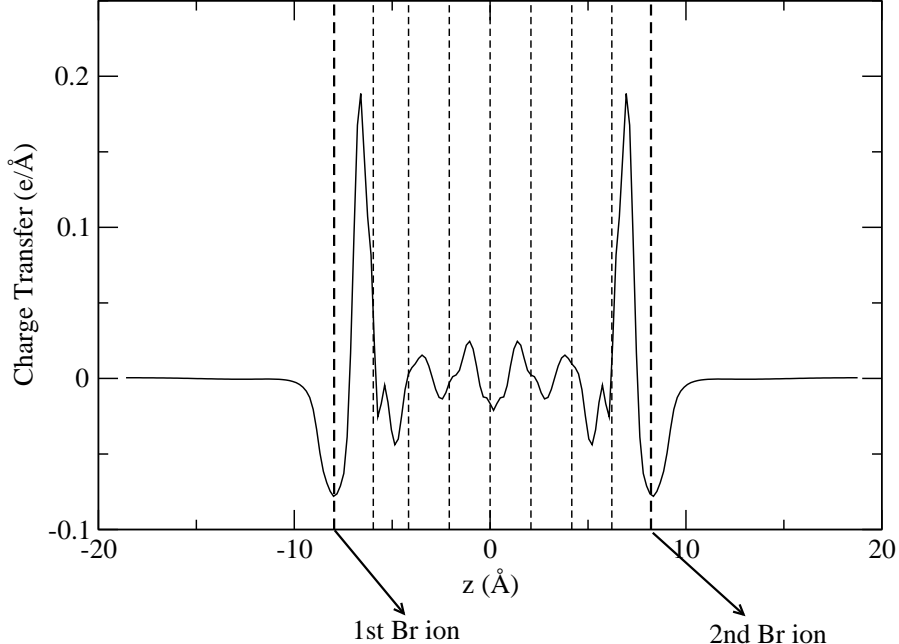


FIG. 4: The charge transfer function  $\Delta\rho(z)$  for Br/Ag(100) with  $\theta = 1/9$ . The vertical short-dashed lines indicate the  $z$ -positions of the Ag layers, and the long-dashed ones indicate those of the adsorbate ions.

case, suggesting an important difference between Br/Ag(100) and Cl/Ag(100). Figure 6, which shows the charge transfer function for low and high coverages, illustrates the difference more clearly. Here we see that there is no significant difference between Br/Ag(100) and Cl/Ag(100) for  $\theta = 1/9$ , while for  $\theta = 1/2$  we see a quite significant difference.

### III. DIPOLE-DIPOLE INTERACTION

In the previous section we have shown that once we have obtained the charge transfer function, we can calculate the dipole moment  $p$  from Eq. (5). Kohn and Lau [24] showed that the non-oscillatory part of the dipole-dipole interaction energy between the adatoms behaves as

$$\phi_{\text{dip-dip}} = \frac{2p_A p_B}{4\pi\epsilon_0 R^3}. \quad (6)$$

The novel aspect of this expression is the factor of 2. A qualitative explanation for this factor is given in Appendix B. For a more detailed and general treatment we refer the reader to Ref. [24]. With Eq. (6), we can calculate  $\phi_{\text{dip-dip}}$  from the surface dipole moment results

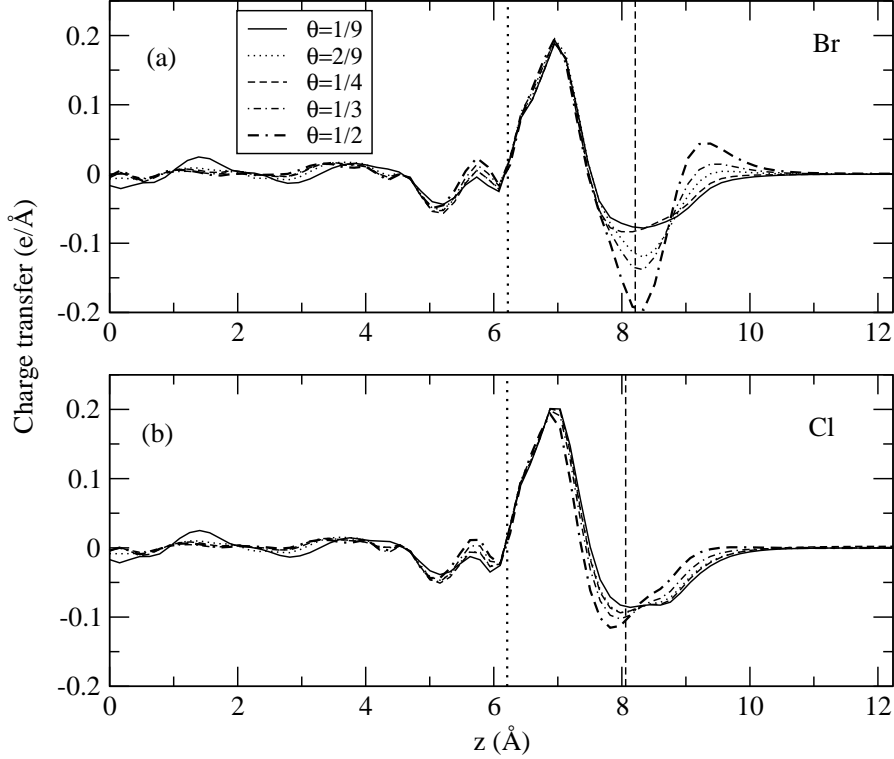


FIG. 5: Charge transfer functions  $\Delta\rho(z)$  for all coverages. Only half of the supercell is shown, from  $z = 0\text{\AA}$  to  $z = 12.235\text{\AA}$ . Panel (a) is for Br/Ag(100) and (b) for Cl/Ag(100). The dotted lines correspond to the  $z$ -position of the topmost layer of metal and the dashed lines correspond to the  $z$ -position of the adsorbates.

from the DFT as described in Eq. (5) as

$$\phi_{\text{dip-dip nnn}} = \frac{2p^2}{4\pi\epsilon_0 R_{\text{nnn}}^3}, \quad (7)$$

for large  $R$  (in our case larger than the nearest-neighbor distance). Here  $p$  is the surface dipole moment calculated from the charge transfer function (Eq. (5)), and  $R_{\text{nnn}}$  is the lateral distance between a pair of next-nearest neighbor adatoms.

#### IV. LATTICE-GAS MODEL

We use an  $L \times L$  square array of  $N_{\text{site}} = L^2$  adsorption sites. Each site corresponds to a four-fold hollow site on the Ag(100) surface. The energy of this lattice-gas model is

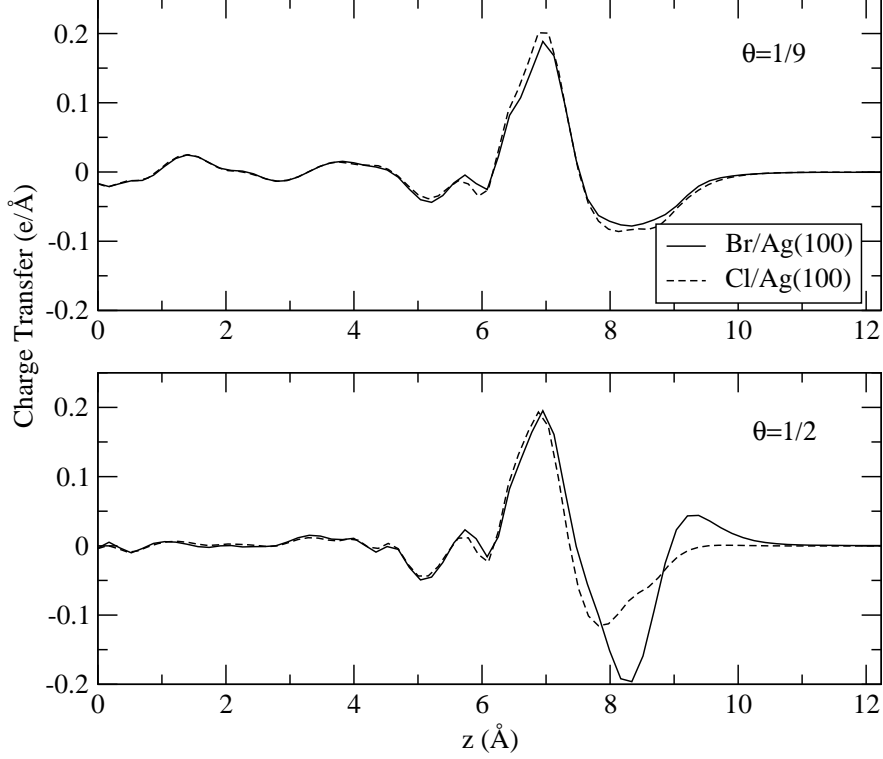


FIG. 6: Comparison of charge transfer functions  $\Delta\rho(z)$  for for Br and Cl at two different coverages.

$$E = - \sum_{i < j} \phi_{ij} c_i c_j - E_b \sum_i^{N_{\text{site}}} c_i. \quad (8)$$

Here  $i$  and  $j$  denote adsorption sites,  $\phi_{ij}$  is the lateral interaction energy of the pair  $(ij)$ , and  $E_b$  is the single-particle binding energy. The sign convention is that  $\phi_{ij} < 0$  signifies repulsive interaction and  $E_b > 0$  favors adsorption [10].  $\sum_{i < j}$  is a sum over all pairs of sites, and  $N_{\text{site}}$  is the number of four-fold hollow sites on each side of the slab. For simplicity we ignore multiparticle interactions [11, 12].

Koper [4] has shown that the effects of screening and finite nearest-neighbor repulsion are very small. Following his results, we use a lattice-gas model with nearest-neighbor exclusion and unscreened dipole-dipole interactions. The distances used in the lattice-gas model are  $R_{ij} = r_{ij}a$  and  $R_{\text{nnn}} = \sqrt{2}a$ , where  $R_{ij}$  is the distance between a pair of adsorbates  $ij$ , and  $a$  is the Ag(100) lattice spacing. We can then write

$$\phi_{ij} = \frac{R_{\text{nnn}}^3}{R_{ij}^3} \phi_{\text{nnn}} = \frac{(\sqrt{2})^3}{r_{ij}^3} \phi_{\text{nnn}}. \quad (9)$$

Thus we have

$$\frac{1}{N_{\text{site}}} \sum_{i<j} \phi_{ij} c_i c_j = \phi_{\text{nnn}} \Sigma_{\theta}, \quad (10)$$

where

$$\Sigma_{\theta} = \frac{(\sqrt{2})^3}{N_{\text{site}}} \sum_{i<j} \frac{c_i c_j}{r_{ij}^3}. \quad (11)$$

The adsorption energy defined in Eq. (2) is related to the lattice-gas energy of Eq. (8) as

$$E_{\text{ads}} = \frac{E}{N_{\text{site}}}. \quad (12)$$

This enables us to break down  $E_{\text{ads}}$  into its lateral-interaction and single-atom binding parts as follows,

$$E_{\text{ads}} = -\phi_{\text{nnn}} \Sigma_{\theta} - E_{\text{b}} \theta, \quad (13)$$

where  $\theta$  is the coverage (Eq. (1)) as before. The subscript  $\theta$  in  $\Sigma_{\theta}$  signifies that the lateral interaction energy is coverage dependent.

Using the supercell set-up of the DFT, the lateral part of Eq. (8) will be the lateral interaction energy per supercell surface. We can calculate this energy by extending the supercell to infinity in the  $x$  and  $y$  directions by means of periodic boundary conditions. The central supercell is the original supercell, and the image supercells are the supercell extensions in the  $x$  and  $y$  directions. The lateral energy per supercell is the sum of the interaction energies of pairs in the central supercell and the lateral energies of pairs of adsorbates in the central supercell and adsorbates in the image supercells. Figure 7(a) shows an example of the lateral energy calculation for  $\theta = 1/9$  for finite  $N_{\text{site}}$ .

The lateral energy per supercell can be written as

$$\Sigma_{\theta} = \sum^{N_{\text{site}}} \frac{C}{r^3}, \quad (14)$$

where  $C$  is an arbitrary constant. The above sum can be approximated by the integral

$$\Sigma_{\theta}(L) \approx \int_0^{2\pi} \int_{L_0}^L \frac{C}{r^3} r dr d\theta, \quad (15)$$

which gives us

$$\Sigma_{\theta}(L) \approx \frac{C_1}{L} + C_2. \quad (16)$$

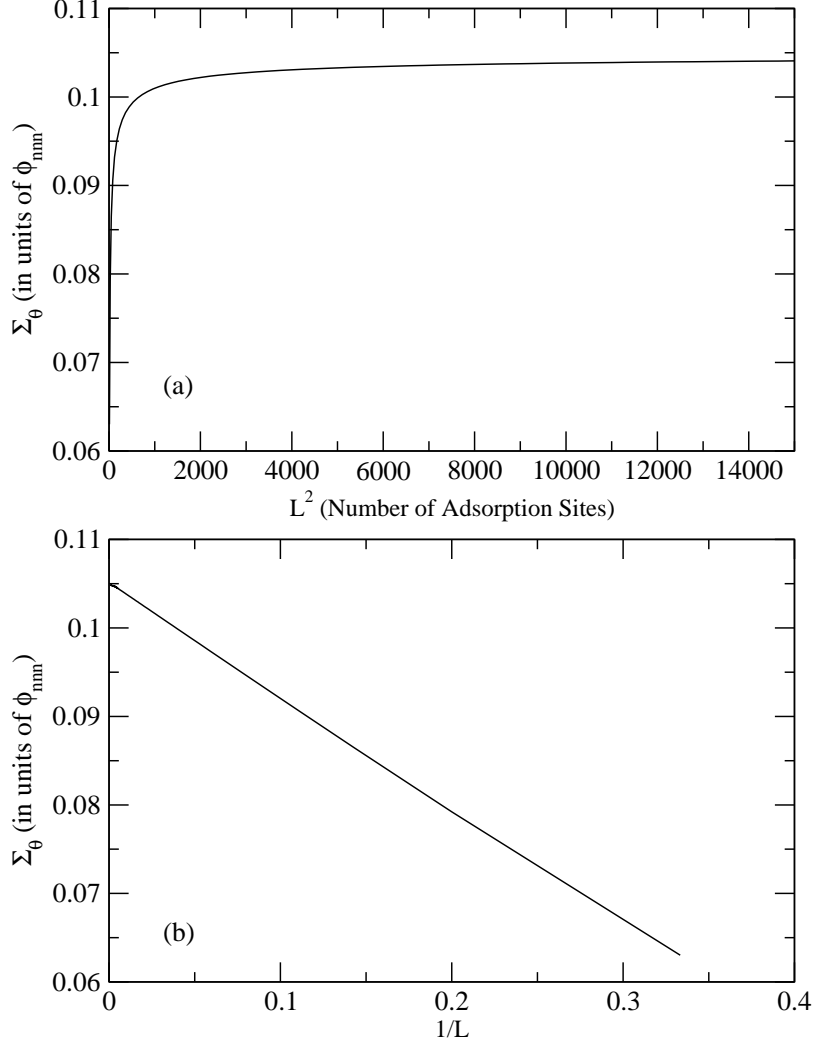


FIG. 7: (a) The lateral energy per supercell as a function of the number of adsorption sites ( $N_{\text{site}} = L^2$ ). As  $L^2$  is increased, the lateral energy approaches an asymptotic value that can be found by plotting the energy per supercell as a function of  $1/L$  and extrapolating the graph to  $1/L = 0$  as shown in (b).

We therefore plot  $\Sigma_\theta$  versus  $1/L$ . It is shown in Fig. 7(b) that the plot is linear in accordance with Eq. (16). The correct lateral energy per supercell can then be obtained by fitting Eq. (16) to the  $\Sigma_\theta$  versus  $1/L$  plot and extrapolating to  $1/L = 0$ . The results of this calculations for the different coverages are presented in Table I.

TABLE I: Lateral interaction energy calculation extrapolated to  $L \rightarrow \infty$ .  $\Sigma_\theta$  is the full lateral interaction energy in units of  $\phi_{\text{nnn}}$ , the lateral energy between a pair of next-nearest neighbors.

$\theta$	$\Sigma_\theta(L \rightarrow \infty)$
1/9	0.10512
2/9	0.58591
1/4	0.79822
1/3	1.53990
1/2	4.26730

## V. LATTICE-GAS FITTING

According to our assumption,  $\phi_{ij}$  is quadratic in  $p$  and  $\sim 1/r^3$ . The  $\sim 1/r^3$  part has already been calculated in  $\Sigma_\theta$  as described in Eqs. (11) and (14-16). We also know from the DFT results that the dipole moment  $p$  is approximately linear in  $\theta$  as shown in Fig. 3. Hence, based on Eq. (7) it is reasonable to assume that we can write  $\phi_{\text{nnn}}$  as [9]

$$\phi_{\text{nnn}} = A(1 + B\theta)^2 \quad (17)$$

From Eqs. (17) and (13), we have three parameters to be extracted:  $A$ ,  $B$ , and  $E_b$ . In Fig. 2 it is shown that  $E_{\text{ads}}$  vs  $\theta$  is predominantly linear. The linear part is proportional to  $E_b$ . The lateral energies contribute to the nonlinear parts which are much weaker, and therefore difficult to estimate accurately from a direct three-parameter fit. We therefore used the following two-step procedure. As can be seen in fig. 2, the graphs extrapolate to  $E_{\text{ads}}(\theta = 0) = 0$ , consistent with the fact that at a very low coverage the lateral energy approaches zero. To obtain the dominant linear coefficient  $E_b$ , we first fit a quadratic equation to  $E_{\text{ads}}(\theta)$ ,

$$E_{\text{ads}}(\theta) = a_0 + a_1\theta + a_2\theta^2. \quad (18)$$

We extracted the linear part  $a_0 + a_1\theta$  and used  $a_1$  as our estimate for the linear coefficient  $E_b$ , finding  $E_b = 3.059 \pm 0.058$  eV for Bromine and  $E_b = 3.371 \pm 0.058$  eV for Chlorine. We then fixed  $E_b$  in Eq. (13) and applied a two-parameter fit to extract  $A$  and  $B$ , which enabled us to calculate  $\phi_{\text{nnn}}$ . (The parameters  $a_0$  and  $a_2$  are complicated functions of  $A$  and

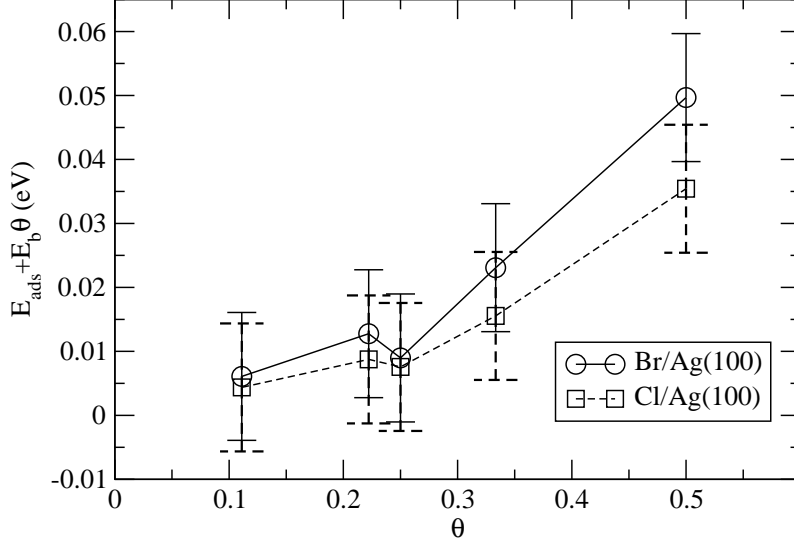


FIG. 8: The contributions of the lateral interactions to  $E_{\text{ads}}$ , shown vs  $\theta$ .

$B$  and were discarded in favor of the direct two-parameter fit of the latter.)

Using  $E_b$  from above, we calculate the contribution of the lateral interactions to  $E_{\text{ads}}$  as

$$C(\theta) = E_{\text{ads}}(\theta) + E_b\theta. \quad (19)$$

In Fig. 8 we plot Eq. (19). From this figure it is obvious that the lateral energy terms are important. Figure 9 shows the fitting results for  $\phi_{\text{nnn}}$ . It is shown in the figure that for Br the lattice-gas model obtained by fitting to the adsorption energies from the DFT calculation is consistent with long-range dipole-dipole lateral interactions using the dipole moments calculated from the DFT charge distribution. This indicates that long-range dipole-dipole interactions are dominant in this system. For Cl the figures show that the long-range dipole-dipole interactions are important but not dominant.

We further note that for low coverages our estimates of  $\phi_{\text{nnn}}$  for Br are in excellent agreement with those obtained by fitting Monte Carlo simulation results for the lattice-gas model to electrochemical adsorption isotherms in Ref. [8]. However, the DFT results show a stronger coverage dependence than obtained from the experimental Monte Carlo fits. The experimental fitting results for Cl from Ref. [9] lie between the two DFT estimates, and all three results show approximately the same coverage dependence.

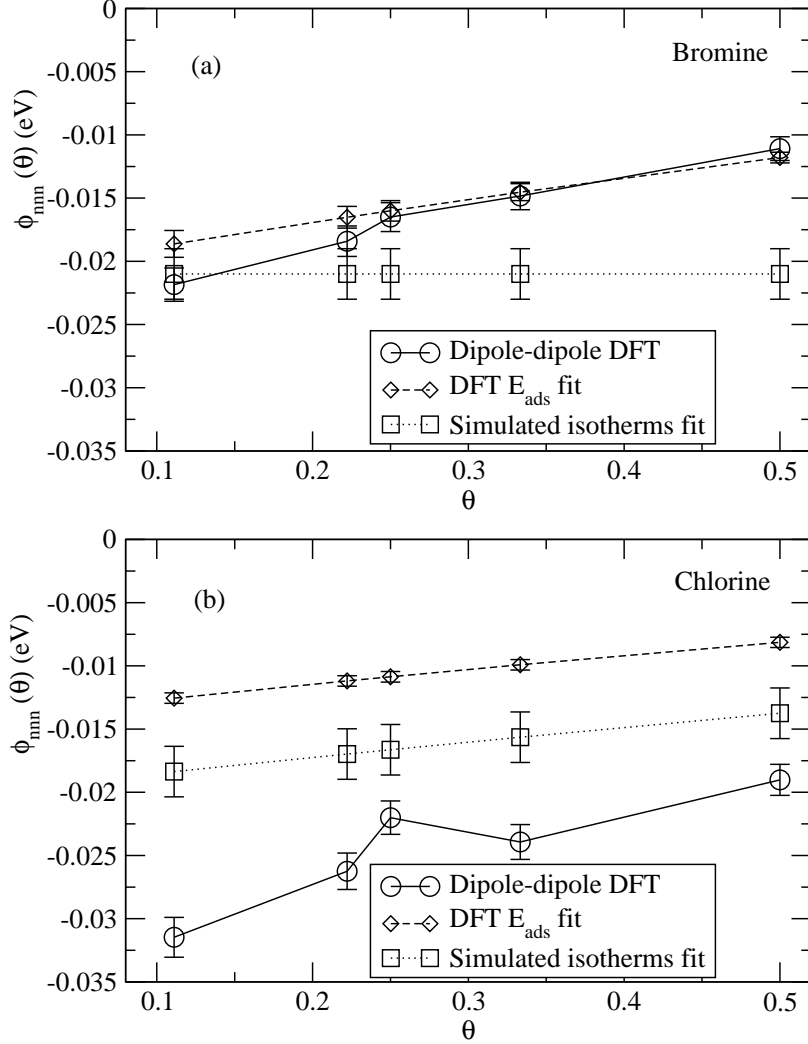


FIG. 9: Comparison of the estimates of  $\phi_{\text{nnn}}$  from lattice-gas fit to the adsorption energies (diamonds) and from the dipole-dipole interactions (circles). Also shown are the results of fitting room-temperature Monte Carlo simulations to electrochemical adsorption isotherms from Refs. [8, 9] (squares). (a): Bromine. (b): Chlorine.

## VI. DISCUSSION

The lattice-gas model in our study consists of two terms, the lateral interaction term and the single-atom binding-energy term. By fitting the lattice-gas model to adsorption energies obtained from DFT calculations, we have calculated the total lateral energy of the systems. From the charge distribution results from DFT, we have calculated the long-range dipole-dipole interaction contribution to the lateral energy terms that falls off as  $\sim 1/r^3$ . With

this assumption, we calculated dipole-dipole lateral interactions by Eq. (6).

Apart from the difference of magnitude of the dipole moments between Br/Ag(100) and Cl/Ag(100), we find that there are differences in the charge distribution around the adsorbates between Bromine and Chlorine. This is an indication that there are important differences between Br/Ag(100) and Cl/Ag(100).

For Bromine, we showed that the lateral energy calculations from the DFT charge distributions are consistent with the results from fitting the lattice-gas model to the DFT adsorption energies. This shows that in the case of Bromine the lateral energy terms are dominated by long range dipole-dipole interactions. In the case of Chlorine, the lateral energy results from the charge distributions are greater in magnitude than those of Bromine, showing that the long-range dipole-dipole interaction in Cl/Ag(100) is important. However, in the case of Chlorine, we see less consistency between the two methods of calculations. This indicates the presence of significant short-range interactions.

Our calculations were done in vacuum. We note, however, the overall consistency of the vacuum DFT calculations presented here with previous fits of lattice-gas Monte Carlo simulations to electrochemical adsorption isotherms. This suggests that our calculations might be useful to understand these experimental results, in which water is present, as well.

### **Acknowledgments**

P.A.R. dedicates this paper to his long-time friend and collaborator, Andrzej Wieckowski, on the occasion of his 65th birthday.

This work was supported in part by U.S. National Science Foundation Grant No. DMR-0802288 and by The Center for Materials Research and Technology (MARTECH) at Florida State University, and by U.S. Department of Energy Contract No. de-sc0004600 at The University of Tulsa. The DFT calculations were performed at Florida State University's High-Performance Computing Center.

### **Appendix A: Convergence Checks**

The number of metal layers in our DFT simulation was determined by convergence checks. We calculated  $E_{\text{ads}}$  for  $\theta = 1/9$  and  $1/2$ , for 5, 7, and 9 layers with exactly the same

simulation parameter set-up (energy cutoff,  $k$ -points, the thickness of the vacuum regions, etc.). From Table I we see that increasing the number of metal layers from 5 to 7 changed  $E_{\text{ads}}$  for Bromine by less than 1 meV for  $\theta = 1/9$  and less than 10 meV for  $\theta = 1/2$ . Similar observations are also shown in Table II for Chlorine. Increasing the number of metal layers from 5 to 7, changed  $E_{\text{ads}}$  for Chlorine by less than 2 meV for  $\theta = 1/9$  and less than 10 meV for  $\theta = 1/2$ .

We also calculated the surface dipole moments for  $\theta = 1/9$ , and  $1/2$ , for 5, 7, and 9 layers from the above simulations. The convergence check for dipole moments as shown in Table III and IV shows that increasing the number of layers from 7 to 9 did not change the dipole moment significantly.

We calculated the percent errors, defined as follows

$$PE_E = \left| \frac{E_{\text{ads}}(i) - E_{\text{ads}}(j)}{E_{\text{ads}}(j)} \right| \times 100\%, \quad (\text{A1})$$

$$PE_p = \left| \frac{p(i) - p(j)}{p(j)} \right| \times 100\%. \quad (\text{A2})$$

Here,  $PE_E$  is the percent error for adsorption energies  $E_{\text{ads}}$  and  $PE_p$  is the percent error for surface dipole moments. In our calculation  $j = 5$  represents the slab with 5 layers, and  $i = 7, 9$  represent the slabs with 7 and 9 layers, respectively. These percent errors are also shown in Tables I-IV

From these two convergence checks ( $E_{\text{ads}}$  and  $p$ ) we concluded that we need at the very least 5 layers of metal, and we decided to use 7 layers. Taking the highest value of  $E_{\text{ads}}(i) - E_{\text{ads}}(i - 2)$  from 5 to 7 layers, which is 7 meV, we estimate the error bars for  $E_{\text{ads}}$  to be  $\Delta E_{\text{ads}} = \pm 10$  meV and for  $p$  to be  $\Delta p = \pm 0.01 e\text{\AA}$ . Error-bar estimates for  $\phi_{\text{nnn}}$  based on  $\Delta p$  were then calculated by direct error propagation. Error-bar estimates for  $E_{\text{ads}}$  were obtained as those leading to a 10% increase in the  $\chi^2$  of the two-parameter fit.

### Appendix B: The Factor 2 in Eq. (6)

Following Ref. [24], a qualitative explanation for the factor 2 in Eq. (6) can be obtained as follows. Consider an adatom A with induced charge  $q_A$ , at a distance  $z_A$  above the plane surface of a semi-infinite conducting medium, located at  $z = 0$ . The charge-transfer function, integrated over  $x$  and  $y$ , is

TABLE I: Convergence check for the Bromine adsorption energy (in units of eV) with respect to the number of metal layers.

BROMINE				
Metal Layers	Coverage	$E_{\text{ads}}$	$E_{\text{ads}}(i) - E_{\text{ads}}(i - 2)$	$PE_E$
5	1/9	-0.334187984	—	
7	1/9	-0.333754808	0.0004331	0.13
9	1/9	-0.339772195	-0.00601	1.67
5	1/2	-1.475041628	—	
7	1/2	-1.479772329	0.00473	0.32
9	1/2	-1.489228380	-0.00946	0.96

TABLE II: Convergence check for the Chlorine adsorption energy (in units of eV) with respect to the number of metal layers.

CHLORINE				
Layers	Coverage	$E_{\text{ads}}$	$E_{\text{ads}}(i) - E_{\text{ads}}(i - 2)$	$PE_E$
5	1/9	-0.371225625	—	—
7	1/9	-0.370121449	0.001104	0.29
9	1/9	-0.376717001	-0.005491	1.48
5	1/2	-1.642027259	—	—
7	1/2	-1.649943352	-0.007916	0.48
9	1/2	-1.730707884	-0.080765	5.40

$$\Delta\rho_A(z) = -q_A\delta(z) + q_A\delta(z - z_A), \quad (\text{B1})$$

where  $\delta(z)$  is the Dirac delta function. This yields the dipole moment,

$$p_A = \int_{-\infty}^{\infty} z\Delta\rho(z)dz = -q_A \cdot 0 + q_A z_A = q_A z_A \quad (\text{B2})$$

This is the physical dipole created by adatom A. However, the electrostatic potential at a point  $z_B$ , a lateral distance  $R \gg z_A$  from A, is that of the dipole formed by  $q_A$  and its image charge  $-q_A$  at  $z = -z_A$ ,

TABLE III: Convergence check for the Bromine surface dipole moment (in units of eÅ) with respect to the number of metal layers.

BROMINE				
Layers	Coverage	$p$	$p(i) - p(i - 2)$	$PE_p$
5	1/9	-0.241532	—	—
7	1/9	-0.166162	0.075369	31.20
9	1/9	-0.178799	-0.012637	25.97
5	1/2	-0.124252	—	—
7	1/2	-0.118376	0.005876	4.72
9	1/2	-0.120788	-0.002412	2.78

TABLE IV: Convergence check for the Chlorine surface dipole moment (in units of eÅ) with respect to the number of metal layers

CHLORINE				
Layers	Coverage	$p$	$p(i) - p(i - 2)$	$PE_p$
5	1/9	-0.267334	—	—
7	1/9	-0.199436	0.067898	25.39
9	1/9	-0.209752	-0.010316	21.54
5	1/2	-0.148922	—	—
7	1/2	-0.155043	-0.006121	4.11
9	1/2	-0.151803	0.003239	1.93

$$U_A(z_B, R) = 2z_A q_A \frac{z_B}{4\pi\epsilon_0 R^3}, \quad (\text{B3})$$

for  $z_B \geq 0$ . This is equivalent to the potential of a fictitious dipole of magnitude  $2z_A q_A = 2p_A$ , twice the magnitude of the physical dipole in Eq. (B2).

An adatom B with induced charge  $q_B$  at  $z_B$  corresponds to the charge transfer function

$$\Delta\rho_B(z) = -q_B\delta(z) + q_B\delta(z - z_B), \quad (\text{B4})$$

which gives  $p_B = q_B z_B$ .

The potential energy of the pair of adatoms is then

$$\begin{aligned}
 U_{AB} &= \int_{-\infty}^{+\infty} U_A(z, R) \Delta\rho_B(z) dz \\
 &= -q_B U_A(0, R) + q_B U_A(z_B, R) \\
 &= 0 + \frac{2z_A q_A z_B q_B}{4\pi\epsilon_0 R^3} \\
 &= \frac{2p_A p_B}{4\pi\epsilon_0 R^3},
 \end{aligned} \tag{B5}$$

which is Eq. (6). In Ref. [24] it is shown that this result holds in more general situations as well, such as jellium and crystalline metals.

- 
- [1] B. Ocko, J. Wang, Th. Wandlowski, Phys. Rev. Lett. 79 (1997) 1511.
  - [2] T. Wandlowski, J. Wang, B. Ocko, J. Electroanal. Chem. 500 (2001) 418.
  - [3] K. Kleinherbers, E. Janssen, A. Goldmann, H. Saalfeld, Surf. Sci. 215 (1989) 394.
  - [4] M. T. M. Koper, J. Electroanal. Chem. 450 (1998) 189.
  - [5] S. Wang, P. A. Rikvold, Phys. Rev. B 65 (2002) 155406.
  - [6] T. Kramar, D. Vogtenhuber, R. Podlucky, A. Neckel, Electrochim. Acta 40 (1995) 43.
  - [7] S. J. Mitchell, S. W. Wang, P. A. Rikvold, Faraday Disc. 121 (2002) 53.
  - [8] I. Abou Hamad, T. Wandlowski, G. Brown, P. A. Rikvold, J. Electroanal. Chem. 554 (2003) 211.
  - [9] I. Abou Hamad, S. Mitchell, T. Wandlowski, P. A. Rikvold, G. Brown, Electrochim. Acta 50 (2005) 5518.
  - [10] S. J. Mitchell, G. Brown, P. A. Rikvold, J. Electroanal. Chem. 493 (2000) 68.
  - [11] T. J. Stasevich, T. L. Einstein, S. Stolbov, Phys. Rev. B 73 (2006) 115426.
  - [12] Y. Tiwary, K. A. Fichthorn, Phys. Rev. B 75 (2002) 235451.
  - [13] D.-J. Liu, Phys. Rev. B 81 (2010) 035415.
  - [14] G. Kresse, J. Hafner, Phys. Rev. B 47 (1993) 558.
  - [15] G. Kresse, J. Furthmüller, Phys. Rev. B 54 (1996) 11169.
  - [16] G. Kresse, J. Furthmüller, Comp. Mat. Sci 6 (1996) 15.
  - [17] J. Perdew, Y. Wang, Phys. Rev. B 45 (1992) 13244.

- [18] J. Perdew, J. Chevary, S. Vosko, K. Jackson, M. Pederson, D. Singh, C. Fiolhais, Phys. Rev. B 46 (1992) 6671.
- [19] D. Vanderbilt, Phys. Rev. B 41 (1990) 7892.
- [20] G. Kresse, J. Hafner, J. Phys.: Condens. Matter 6 (1994) 8245.
- [21] H. Monkhorst, J. Pack, Phys. Rev. B 13 (1976) 5188.
- [22] S. J. Mitchell, M. T. M. Koper, Surf. Sci. 563 (2004) 169.
- [23] T. C. Leung, C. L. Kao, W. S. Su, Y. J. Feng, C. T. Chan, Phys. Rev. B 68 (2003) 195408.
- [24] W. Kohn, K. Lau, Sol. State Commun. 18 (1976) 553.